Biogeosciences Discussions

Biogeosciences Discussions is the access reviewed discussion forum of *Biogeosciences*

Alkenone-like proxy record in the NW African upwelling

X. Giraud

Modelling an alkenone-like proxy record in the NW African upwelling

X. Giraud

Research Center Ocean Margins, Universität Bremen, Postfach 330 440, 28 334 Bremen, Germany

Correspondence to: X. Giraud (xgiraud@palmod.uni-bremen.de)

Title Page

Abstract	Introduction
Conclusions	References
Tables	Figures

◄◄ ►►

◄ ►

Back Close

Full Screen / Esc

Print Version

Interactive Discussion

EGU

Abstract

A regional biogeochemical model is applied to the NW African coastal upwelling between 19° N and 27° N to investigate how a water temperature proxy is produced at the sea surface and recorded in the slope sediments. The biological model has two phytoplankton groups, to distinguish an alkenone producer group (considered as coccolithophores) from other phytoplankton. The Regional Ocean Modelling System (ROMS) is used to simulate the ocean circulation, and takes advantage of the Adaptive Grid Refinement in Fortran (AGRIF) package to set up an embedded griding system. The results show that the alkenone-like temperature records in the sediments are between 1.1 and 2.1°C colder compared to the annual mean SSTs. Despite the seasonality of the coccolithophorid production, this temperature difference is not mainly due to a seasonal bias, nor to the lateral advection of phytoplankton and phytodetritus from the cold water domain to most offshore locations, but to the production depth of the coccolithophores. If core-top sediment alkenone-derived temperatures are effectively recording the annual mean SSTs, the quantitative alkenone production in the water column must be inhomogeneous among the coccolithophore population and depend on physiological factors (growth rate, nutrient stress).

1. Introduction

A large number of paleoceanographic studies use the alkenone ratio in sediments to reconstruct past sea surface temperatures (SSTs) (e.g. Zhao et al., 2000; Sicre et al., 2000, 2001; Sachs and Anderson, 2003). This approach is based on the discovery that the relative content of long-chain (C_{37}) unsaturated ketones (alkenones) in certain Haptophyte algae, especially the coccolithophores *Emiliania huxleyi* and species of the genus *Gephyrocapsa*, depends on the growth temperature of these algae (Marlow, 1984; Brassell et al., 1986; Conte et al., 1998). Prahl et al. (1988) calibrated a linear relation between an unsaturation alkenone index (Uk'37) and the growth temperature

EGU

of an *E. huxleyi* strain in culture experiments. It has been then confirmed that this tool could be used in open ocean to reconstruct SSTs from core top sediment measurements (Müller et al., 1998).

In order to be used as a paleoproxy, the Uk'37 has to fulfil certain criteria. The stabil-
⁵ ity of the Uk'37 signal during water column degradation and sedimentary diagenesis is still a question. Some contradictory results argue for a modification of the original temperature signal (Hoefs et al., 1998; Gong and Hollander, 1999; Rontani et al., 2005), whereas other studies conclude that there is no diagenetic effect on the temperature record (e.g. Grimalt et al., 2000; Harvey, 2000). The species considered as the main
¹⁰ alkenone producer and who served for the temperature-dependence calibration, *E. huxleyi*, is widely distributed in the present day world ocean. The calibration has also been confirmed for other alkenone-producer species prior to the apparition of *E. huxleyi* (Conte et al., 1998). Finally, the global core top calibration of Müller et al. (1998), as well as other regional studies (e.g. Prahl et al., 2005), have established that the
¹⁵ alkenone index was best correlated with the annual mean SSTs. Thus the alkenone proxy is widely used to reconstruct paleo annual mean SSTs.

Nevertheless, the relationship between Uk'37 and annual mean SSTs may be biased by different factors, particularly by the conditions of generation, transport and burial of the alkenones. The seasonality of alkenone producers causes in certain regions a bias
²⁰ toward springtime (Conte et al., 1992) or winter period (Herbert et al., 1998). The depth of maximum alkenone concentration is not necessarily located at the sea surface, but corresponds to the depth of maximum chlorophyll concentration, and varies from the surface to sub-surface (Lee and Schneider, 2005). The lateral advection of particles or resuspension and transport of sediments on long distances by strong surface or bottom
²⁵ currents may produce mismatches between the alkenone derived temperatures and the SSTs (e.g. Benthien and Müller, 2000).

These considerations have lead to the notion of Integrated Production Temperature (IPT, Conte and Eglinton, 1993; Conte et al., 1998). The alkenone content of the sediments reflects the integrated production over years, including the annual seasonality

and the interannual variability, for which the spatial origin varies with the advection and mixing processes, and modified by differential losses in the water column or by diagenetic processes. The challenge for a good use of a paleo-proxy consists to have an accurate picture of the full path of processes responsible for its production and settling.

5 The IPT is therefore the temperature record in sediments, after the integration of all processes of production, transport and transformation, and is therefore not necessarily the above annual mean SST. The notion of IPT can be extended to other temperature proxy, like Mg/Ca ratio in foraminiferal tests or statistical assemblages, since the planktonic rests may also experience the advection/transport processes or a preferential

10 seasonal production.

The present study aims to reconstruct the alkenone-derived IPT in the context of the North West African coastal upwelling by a modelling approach, to compare the modelled IPT with SSTs and alkenone derived temperatures from core top sediments, and to evaluate the potential biases. A biogeochemical model has been developed to

15 consider the production and settling of an alkenone-like temperature proxy. This implies to consider an alkenone producer phytoplankton pool separated from the rest of the primary producers, in order to capture the time and space distribution of the alkenones production. It has been coupled to a regional ocean circulation model and applied to the NW Africa coastal upwelling, centred on the Mauritanian coast, between $19°$ N

20 and $27°$ N. The two models are presented in Sect. 2. Section 3 presents the results. In Sect. 4, we discuss the influence of the seasonality, production depth, lateral and vertical advection of phytoplankton and phytodetritus, and the sediment resuspension, before to conclude in Sect. 5.

EGU

2. Model description and simulations set up

2.1. Physical model

2.1.1. Background

The ocean circulation model is the Regional Ocean Modelling System (ROMS). ROMS solves the primitive equations based on Boussinesq and hydrostatic approximations, with a free surface, horizontal curvilinear coordinates, and using a terrain following (sigma coordinates) vertical curvilinear grid. A complete description can be found in Shchepetkin and McWilliams (2003, 2005). ROMS has been applied in different regional modelling studies, and in particular in coastal upwelling systems (Blanke et al., 2002; Marchesiello et al., 2003; Di Lorenzo et al., 2004).

We are using a nesting approach in order to perform a high-resolution modelling on the NW Africa margin. A low resolution grid is set up on an extended domain, between 15° N and 32° N, so called the parent grid, and a higher resolution embedded grid, or child grid, is centred on the study area, between 19° N and 28° N (Fig. 1). This embedded griding takes advantage of the AGRIF (Adaptive Grid Refinement in Fortran) package (Blayo and Debreu, 1999; Debreu, 2000; Debreu and Vouland, 2003). The refinement between the parent and the child grids is set to a factor 3. This is applied to the resolution and the time stepping. Therefore, the parent and the child grids have a resolution of 1/5° and 1/15°, respectively. The baroclinic time steps are 1800s and 600s for the parent and child grids, respectively. The number of barotropic time-steps between each baroclinic time-steps is set to 45. The vertical grid has 20 levels with a surface and bottom refinement using the stretching parameters θ_s=4.5 and θ_b=0.9 to allow for a good representation of surface and bottom boundary layers.

The topography is obtained by linear interpolation of the GEBCO Digital Atlas published by the British Oceanographic Data Centre (BODC) on behalf of IOC and IHO (IOC, IHO and BODC, 2003). Depths shallower than 10 m are reset to 10 m. The topography is smoothed with a maximum slope parameter (r=$grad\,(h)\big/h$, where h is the

Alkenone-like proxy record in the NW African upwelling

X. Giraud

Title Page

Abstract	Introduction
Conclusions	References
Tables	Figures

◄◄   ►►

◄   ►

Back   Close

Full Screen / Esc

Print Version

Interactive Discussion

EGU

depth) of 0.2.

2.1.2. Forcing and initial conditions

The model has been initialized using the temperature and salinity fields from Levitus et al. (1994) and Levitus and Boyer (1994) for the month of January, and no flow. A monthly climatology for the open boundaries has been produced using the World Ocean Atlas (Levitus et al., 1994; Levitus and Boyer, 1994) temperature and salinity and the Comprehensive Ocean-Atmosphere Data Set (COADS) (da Silva et al., 1994) winds, assuming a level of no motion at 2000 m to determine the total velocity. See also Marchesiello et al. (2003) and references therein for a description of the boundary conditions. The surface forcing is provided by mean-seasonal heat and fresh-water flux derived from the COADS. The wind forcing is issued from the daily re-analysis of the European Centre for Medium-range Weather Forcasts (ECMWF) dataset by Röske (2001) for the purpose of the Ocean Model Intercomparison Project (OMIP).

2.2. Biological model

The most abundant coccolithophore species, *Emiliana huxleyi* and *Gephyrocapsa oceanica*, are also though to be the main producers of alkenones in the present ocean (Volkman et al., 1995). In view of the SST record modelling using an alkenone-like proxy, the origin of this biomarker implies to consider an alkenone-producer pool, hereafter assimilated to the coccolithophores. Since not all phytoplankton groups produce alkenones, and since coccolithophores do not necessarily represent a constant proportion of the total phytoplankton, the coccolithophores should be distinguished from the other phytoplankton pool, which includes the non-alkenone producers (diatoms, flagellates...).

EGU

2.2.1. Initial NPPZD model

The biological model used for this study is derived from the NPZD model described by Oschlies and Garçon (1999) and Giraud et al. (2000, 2003). The phytoplankton pool has been divided in two plankton functional types (PFTs). The two phytoplanktonic PFTs (P_1 and P_2) have different growth rate parameters, which leads to different behaviours during the productive phase of the upwelling. One PFT has characteristics close to a diatom pool (P_1, hereafter considered as diatoms), whereas the second one is parameterized with coccolithophorid values (P_2, hereafter also called coccolithophores).

The basic structure of the ecosystem model is therefore a five component, nitrogen based model (Fig. 2, left part), in which individual biological tracers, namely nutrients (N), diatoms (P_1), coccolithophores (P_2), zooplankton (Z) and detritus (D), follow the source-minus-sink terms presented by the following differential equations:

$$dP_1/dt = J_1(z,t,N)P_1 - \frac{P_1}{P_1+P_2}G(P_1+P_2)Z - \mu_P P_1 \tag{1}$$

$$dP_2/dt = J_2(z,t,N)P_2 - \frac{P_2}{P_1+P_2}G(P_1+P_2)Z - \mu_P P_2 \tag{2}$$

$$dZ/dt = \gamma_1 G(P_1+P_2)Z - \gamma_2 Z - \mu_Z Z^2 \tag{3}$$

$$dD/dt = (1-\gamma_1)G(P_1+P_2)Z + \mu_P(P_1+P_2) + \mu_Z Z^2 - \mu_D D \tag{4}$$

$$dN/dt = \mu_D D + \gamma_2 Z - J_1(z,t,N)P_1 - J_2(z,t,N)P_2 \tag{5}$$

where G is the zooplankton grazing function, and J is the phytoplankton growth rate as a function of depth z and time t. The five N–P_1–P_2–Z–D state variables are expressed in mmol N m^{-3}, and parameters and functions are presented in Table 1. The grazing function G is calculated considering the total phytoplankton concentration, and

EGU

is applied to P_1 and P_2 according to their relative proportion. The short wave radiations are provided by the COADS monthly climatology, with a 5° resolution, and follow a reconstructed diurnal cycle.

The phytoplankton growth rate function J is applied identically to the PFTs P_1 and P_2. The difference lies in the parameterisation of the maximum growth rate and the half saturation constant for nitrate uptake. These parameters drive the competitive ability of each PFT relative to the over one. The Table 2 presents a short compilation of these parameters from other PFT biogeochemical models or laboratory experiments. A generic maximum growth rate value of $0.6\,d^{-1}$ is widely used for phytoplankton in biogeochemistry models (Le Quéré et al., 2005), and is the value used for the initial NPZD model (Oschlies and Garçon, 1999; Giraud et al., 2000, 2003). The maximum growth rate for the coccolithophores is usually lower than that of the diatoms, at around two thirds (Eppley et al., 1969; Chai et al., 2002; Gregg et al., 2003). The half saturation constant reflects the ability to use low levels of nutrients, and varies approximately in proportion with cell size and inversely with specific growth rate (Eppley et al., 1969). According to Eppley et al. (1969), the value of this parameter is $\leq 0.5\,mmol\,NO_3\,m^{-3}$ for coccolithophores. Classical values for the half saturation of nitrate uptake are around $0.5\,mmol\,NO_3\,m^{-3}$ for the coccolithophores, and range between 1 and $2.5\,mmol\,NO_3$ m^{-3} for the diatoms (Eppley et al., 1969; Chai et al., 2002; Moore et al., 2002, 2004; Gregg et al., 2003; Le Quéré, 2005). The values adopted for the present model study are similar to the one proposed by E. Buitenhuis in the Dynamic Green Ocean Project (available at http://lgmacweb.env.uea.ac.uk/green_ocean/). The maximum growth rates are set to $0.6\,d^{-1}$ and $0.4\,d^{-1}$, and the half saturation coefficients to 2.1 and 0.53 mmol $NO_3\,m^{-3}$, for diatoms and coccolithophores, respectively. These values are also summarised in the bottom part of Table 2.

An additional sinking term is applied to the detritus pool. In the upwelling context, fecal pellets and organic matter form aggregates having fast sinking velocities. Bory et al. (2001) report settling rates of about $150\,m\,d^{-1}$ at the oligotrophic site of EUMELI program, off Cape Blanc, and suggest much faster settling rates at the mesotrophic site.

Fischer et al. (1996) and Müller and Fischer (2001) also report sinking velocities for the organic matter of the order of $280\,\mathrm{m\,d^{-1}}$ in the same mesotrophic context. Because we have only one detritus pool, and considering that the study area covers eutrophic to oligotrophic conditions, we considered for the reference simulation a constant sinking velocity of $200\,\mathrm{m\,d^{-1}}$.

The nitrate and phytoplankton fields were initialized with the World Ocean Atlas database (Conkright et al., 2002). The total phytoplankton biomass is calculated assuming a chlorophyll-a:N ratio of $1.59\,\mathrm{mg\,chla\,(mmol\,N)^{-1}}$ (Oschlies and Garçon, 1999). The ratio between the initial coccolithophore and diatom concentrations is then set to 0.5, the zooplankton concentration is set to 30% of the total phytoplankton, and there is no detritus or phytodetritus.

2.2.2. Modelling an alkenone-like proxy

The basis of the biological model provides the development of the phytoplankton and the loop of the trophic chain. In order to track the alkenone-like proxy from the surface to the bottom, the detritus pool produced by the coccolithophores only has to be distinguished from the total detritus pool (D). The new state variable is therefore a phytodetritus pool (D_2, in $\mathrm{mmol\,N\,m^{-3}}$) having only the coccolithophores (P_2) as a source (Fig. 2, right part). D_2 has the same characteristics as D (remineralization rate, mortality rate and sinking velocity). The source-minus-sink terms of D_2 are given by the following equation:

$$dD_2 \big/ dt = (1 - \gamma_1)\,\frac{P_2}{P_1 + P_2} G\,(P_1 + P_2)\,Z + \mu_P P_2 - \mu_D D_2 \qquad (6)$$

We need also other state variables to carry the information of the temperature at which the coccolithophores grew. The strategy is to run in parallel the state variables giving the concentrations (namely P_2 and D_2, in $\mathrm{mmol\,N\,m^{-3}}$), and two new ones giving the concentration weighted temperature (namely P_{2T} and D_{2T}, in $\mathrm{^\circ C\,mmol\,N\,m^{-3}}$). The

alkenone-like temperatures of the coccolithophores (T_{P2}, in °C) and the phytodetritus (T_{D2}, in °C) are simply retrieved as follow:

$$T_{P2} = P_{2T}/P_2 \tag{7}$$

$$T_{D2} = D_{2T}/D_2 \tag{8}$$

T_{P2} corresponds to the temperature in which the coccolithophorid pool grew, and can be seen as the alkenone-like proxy. T_{D2} is the same alkenone like proxy, but applied to the detritus pool, issued from the coccolithophores death and unassimilated zooplankton grazing part.

The role of the alkenones in the physiology of the coccolithophores is not elucidated. It has been proposed that the alkenones and associated compounds participate to the buoyancy of the cells (Fernandez et al., 1994), somehow regulate the membrane fluidity, or are associated with the formation of coccoliths (Sawada and Shiraiwa, 2004). Some recent studies propose that alkenones are metabolic storage lipids, and that their metabolic utilisation is not a source of error in the temperature estimation (Epstein et al., 2001; Sawada and Shiraiwa, 2004). Whatever the physiological role of alkenones, the point of interest for the present modelling purpose is the rate of turn over of these compounds.

Conte et al. (1998) concluded that the alkenone composition adapts rapidly to the environmental conditions, even in stressed populations, and that these compounds turn over rapidly. As a basic assumption for the coming reference simulation, we assume that the alkenone ratio in the phytoplankton pool is permanently adapted to the surrounding water temperature (T_w), so that at any time $T_{P2}=T_w$.

But it has been also suggested that the way of production of the alkenones is a constant addition of "new" alkenones to an older stock (Epstein et al., 1998). A consequence would be a certain delay in the answer of the phytoplankton pool to rapid changes in the environmental conditions. In this particular case, the difficulty lies in the estimation of the rapidity of adaptation. Following the view of Epstein et al. (1998),

Alkenone-like proxy record in the NW African upwelling

X. Giraud

Title Page

Abstract | Introduction

Conclusions | References

Tables | Figures

◄ | ►

◄ | ►

Back | Close

Full Screen / Esc

Print Version

Interactive Discussion

EGU

we set up an additional equation, considering that the temperature record of the coccolithophores adapt to the local water temperature only during the growing phase, by production of new mater and incorporation to the older stock. The new equation drives the concentration weighted temperature of the coccolithophores as follow:

$$dP_{2T}/dt = J_2(z, t, N) P_2 T_w - \frac{P_2}{P_1 + P_2} G(P_1 + P_2) ZT_{P2} - \mu_P P_2 T_{P2} \qquad (9)$$

and is going to be used in simulations in parallel to the reference one. Equation (9) shows that the P_{2T} pool grows proportionally to the coccolithophorid primary production ($J_2 P_2$) and to the local temperature of the water (T_w). At any time, this pool is therefore a mixing of concentration weighted temperature from different origins, cumulating in time. But the influence of the former production is progressively removed by the processes of mortality and zooplankton grazing, and transmitted to the phytodetritus pool (D_{2T}).

Concerning the phytodetritus pool, we consider that the temperature signal carried by the alkenone biomarkers is not modified by any diagenetic process. The variations of D_{2T} are then only due to mixing with other phytodetritus pools and source-minus-sink terms of remineralization and coccolithophores mortality, based on Eq. (6) as follow:

$$dD_{2T}/dt = (1 - \gamma_1) \frac{P_2}{P_1 + P_2} G(P_1 + P_2) ZT_{P2} + \mu_P P_2 T_{P2} - \mu_D D_2 T_{D2} \qquad (10)$$

2.3. Sedimentary production

2.3.1. Sediment transport

The detritus pool is carrying the biogeochemical information from the surface to the sea floor. But its final comparison with the core sediments requires considering further transformation processes.

The detritus reaching the sea floor become sedimentary material, which might be resuspended by bottom currents and transported in the water column. They form bottom boundary layer aggregates, acquiring different properties than the sinking detritus

(Thomsen et al., 2002). In particular, the organic matter may stick to inorganic minerals, so that its remineralization rate is lower.

Therefore we implemented additional state variables to the biological model: the suspended sediments (S) and the associated temperature proxy pools, the phytodetritic suspended sediments (S_2) and its concentration weighted temperature (S_{2T}), originating from the D, D_2 and D_{2T}, respectively (Fig. 2).

As mentioned above, the only sources for the S components come from the D pools accumulating on the sea floor and having been resuspended. The S components are resuspended by the bottom shear stress, with a flux F_S (mmol N m^{-2} d^{-1}) expressed as follow:

$$F_S = F_{BC} + F_{ST} \tag{11}$$

where

$$F_{BC} = K_C \frac{\tau_b - \tau_{CR}}{\tau_{CR}}, \text{ for } \tau_b > \tau_{CR} \tag{12}$$

and

$$F_{ST} = K_S (H_{CR} - H), \text{ for } H < H_{CR} \tag{13}$$

where F_{BC} is the resuspension flux associated with the bottom current stress, K_C and K_S are erosion coefficients (mmol N m^{-2} d^{-1}), τ_b is the bottom shear stress and τ_{CR} is the critical shear stress for the resuspension (both in N m^{-2}). F_{ST} is the resuspension flux associated with the storm events and tides, H is the water depth (m), and H_{CR} is an empirical maximum depth of impact of this resuspension term.

The parameterisation of the resuspension processes is different for each study area (lakes, coastal domain, continental shelves), because of the many sediment types, grain sizes and cohesion properties. Our purpose in this work is to be able to take into account the eventual transport of sediments from the shelf and there influence on the continental slope accumulation, on the seasonal time scale. Fütterer (1983) interprets

EGU

the grain size distribution on the shelf and slope off NW Africa as reflecting the action of currents and waves. The rework and eventual erosion of the shelf let only coarse material on the shelf and upper slope. The maximum organic matter content is located at around 1000 m to 2000 m depth on the slope, off Cape Blanc. Our parameterisation is therefore set up to minimize the sedimentary accumulation of organic matter on the shelf.

The formulation of F_{BC} corresponds to a classical expression of the resuspension flux as a function of the bottom shear stress (Blom and Aalderink, 1998; Ribbe and Holloway, 2001). The critical shear stress τ_{CR} is set to 0.01 N m^{-2}, corresponding to the limit of resuspension for organic material (Peterson, 1999).

The F_{ST} term considers the impact of the tidal currents and storm events, both processes being not explicitly modelled. The present formulation is empirical and the effects are limited to the continental shelf, with a maximum effect for shallow areas, and decrease to be null at 200 m depth (H_{CR}). The K_S is set to 5 mmol m^{-2} d^{-1}, which value is fixed after a few sensitivity experiments in our model. A too high value of this coefficient leads to non negligible resuspension terms in the deep water domain (continental slope or abyssal plain), that seem unrealistic.

The total flux is limited to the amount available in the sediments, and the mass budget is therefore respected. Once in the water column, the S components are advected by the ocean circulation model like other biological state variables. The only sink term, unless the resettling on the sea floor with the same sinking velocity as D, is the remineralization as follow:

$$dS/dt = -\mu_S S \tag{14}$$

Equation (14) is also applied with the same remineralization rate and sinking velocity to the S_2 and S_{2T} components (see also Table 1). Only the remineralization term applied to the S component is going back to the nutrient pool (Fig. 2).

2.3.2. Sediment accumulation over time

The second aspect of the sedimentary production is a long-term transformation. The sediments are made of a material that has accumulated over centuries or millennia. This time scale is out of range with the simulations presented in this work, reproducing only seasonal cycles over a few years at maximum. Considering that our simulations are proposing an averaged picture of a certain time period (Present Day), the realism of the sea surface and column water processes does not suffer of this time gap. But the long term diagenetic processes cannot be explicitly considered. Nevertheless, alkenones are known to be among the most refractory lipids (Grimalt et al., 2000) and many studies suggest that the Uk'37 index is not affected by diagenesis (e.g. Grimalt et al., 2000; Harvey, 2000). Therefore, the only expected effect of the diagenesis is a reduction of the organic matter accumulation, without modification of the temperature-record.

2.3.3. Experimental set up and simulations

The biological model is applied on both parent and child grids, with a time step half of the baroclinic physical time step, and the parent provides the boundary conditions for the child grid. The biological fields exported from the child domain do not influence the parent. This is not a problem since few feedbacks are expected once the water mass flows out of our central study area.

The simulation protocol includes two years of simulation with only the physics on the parent domain, followed by one year of full coupling physics and biology on the embedded grids to achieve a full development and a coherent distribution of the biogeochemical tracers. A fourth year of simulation is then performed to provide the results presented hereafter. In the following figures and results, only the child domain is presented and discussed.

Different simulations were performed. The reference simulation (simulation STD) considers that the alkenone-like temperature of the coccolithophores is always equal

Alkenone-like proxy record in the NW African upwelling

X. Giraud

to the surrounding water temperature. A parallel case considers the inertia of the temperature record in coccolithophores, as discussed in Sect. 2.2.2, and uses Eq. (9). This case is referred hereafter as simulation DELAY. For both of these configurations, a series of sensitivity tests have been performed, to evaluate the impact on the IPT of the advection of particles, detritus sinking rate, or depth production of the coccolithophores. These sensitivity cases are presented and commented in the discussion of Sect. 4.

3. Results

3.1. Hydrography

Figure 3 shows modelling results of SSTs and surface currents in winter and summer. North of Cape Blanc, the coastal surface current flows equatorwards all year long. South of Cape Blanc, the currents flow northward in summer and southward in winter. The upwelling that develops on the continental shelf brings deep cold water to the coast, where SSTs are lower than 17˚C. Offshore SSTs show a strong seasonal pattern, with a warming up to 25˚C in summer, while in winter, the onshore-offshore temperature gradient is only 3–4˚C. The coastal currents form eddy structures that participate to the exchange between coastal and offshore waters. All these patterns are in good agreement with the description given by Mittelstaedt (1991).

The mixed layer depth (MLD) is also an important feature to look at, since it may drive the mixing of the phytoplankton and the influx of deep nutrient in the surface ocean, and therefore influence the primary productivity and the phytoplankton distribution. Figure 4 compares the seasonal MLD of the model with observations (Kara et al., 2002). Data and model results are in good agreement. Only small differences appear in spring and summer at the northern boundary of the domain. We consider that this may not play a major role, since it is a local scale feature, which could not be captured by the 1˚×1˚ resolution of the observations.

3.2. Primary production and coccolithophores distribution

In the reference simulation, the distribution of total phytoplankton concentration resembles the general pattern of a coastal upwelling, with higher concentrations close to the coast, with a maximum of 3.5 mg chla m^{-3} in summer (assuming a chla/N ratio of 1.59 mg chla (mmol N)$^{-1}$ (Oschlies and Garçon, 1999), and considering the total phytoplankton concentration P_1 and P_2). It corresponds to the maximum chlorophyll concentration reported for the Mauritanian upwelling (Fischer et al., 1996; Gabric et al., 1993; Morel, 2000).

The relative distribution of coccolithophores and diatoms is driven by their competitive ability to grow on different levels of nutrient concentrations. This distribution is controlled in the model by the PFT parameterisation used to distinguish the diatoms from the coccolithophores, which is based only on the growth rate and the nitrate assimilation parameters. According to the parameterisation, the diatoms have a higher growth rate than coccolithophores for nitrate concentrations greater than 2.7 mmol NO$_3$ m^{-3}. These conditions occur during the strong upwelling events, i.e. in summer, and close to the coast. In contrast, coccolithophores are favoured in water masses relatively more nitrate depleted, i.e. during the winter period and in more offshore position in summer. The typical succession of phytoplankton communities in upwelling systems is therefore a diatom-dominated structure in the central high nutrient concentration upwelling, followed by flagellates and coccolithophores dominance during the water column stratification (Tilstone et al., 2000; Schiebel et al., 2004).

This sequence of diatoms and coccolithophores is well represented by the model (Fig. 5). The diatoms and coccolithophores show opposite seasonal patterns. The maximum surface concentrations occur in summer for the diatoms and in winter for the coccolithophores (1.29 and 0.51 mmol N m^{-3}, respectively). The diatoms distribution shows a strong contrast between high concentrations at the coast, where SSTs are colder and nutrient concentrations higher, and lower concentrations offshore. The coccolithophores distribution is more spread out, with maximum localised more offshore

compared to the diatom bloom. The maximum of coccolithophore concentration always appears in a secondary stage in the phytoplanktonic sequence associated with the upwelling high primary production.

⁵ Figure 6 shows the model results of seasonal vertical profiles of coccolithophores concentration, phytodetritus concentration, and phytodetritus alkenone-like temperature from simulations STD and DELAY, at core location SU94-11S, at the latitude of Cape Blanc (see Fig. 1 for location). It appears clearly that the coccolithophore production follows a seasonal cycle. The concentration of coccolithophores is twice as much in winter than in summer (Fig. 6a). A similar maximum of coccolithophores in winter ¹⁰ is found in observations at stations CB offshore Cape Blanc (Köbrich and Baumann, 2004; Köbrich, personal communication). At a Canary Island station, the maximum coccolith flux also occurred in winter, when SSTs are at lowest (Bijma et al., 2001; Sprengel et al., 2002). This seasonal pattern is also visible with the phytodetritus concentrations (Fig. 6b). The phytodetritus concentration progressively increases from the ¹⁵ surface to ∼100 m depth, before to slowly decrease with depth due to remineralization.

The vertical distribution of the coccolithophores at core location SU94-11S (Fig. 6a) shows a maximum concentration over the first 30 m in winter, spring and summer, and until 50 m depth in autumn. It then rapidly decreases to zero at ∼200 m. According to this distribution, ∼60% of the coccolithophorid mass is located in the upper ²⁰ 50 m. Time series of coccolithophores standing stocks and taxonomic compositions at the Bermuda Atlantic Hydrostation "S", nearby BATS station, have shown that coccolithophore cell densities were highest in the upper 50 m, and decreased rapidly below 100 m (Haidar and Thierstein, 2001). It indicates also that *E. huxleyi* can present local maximum densities from the surface until 50 m, and be the dominant coccolithophore ²⁵ species until 200 m.

EGU

3.3. Temperature record

3.3.1. Temperature record by phytodetritus in the water column

In the reference simulation STD, the phytodetritus alkenone-like temperatures at the surface are similar to the SSTs (Fig. 6c), which is consistent with the fact that the coccolithophores alkenone-like temperature is always adapted to the surrounding water temperature. The phytodetritus alkenone-like temperature then decreases until the depth of maximum phytodetritus concentration, reflecting the progressive accumulation of the deeper and colder phytodetritus production by the coccolithophores. This temperature decrease is ∼0.8°C in spring and autumn. Below the maximum phytodetritus concentration depth, the alkenone-like temperature carried by the phytodetritus pool slightly decreases in autumn, winter and spring (around −0.2°C from ∼100 m to the bottom), and drops of about 1°C in summer. We consider that these variations at great depth are due to the unequal quantity of phytodetritus reaching depth, in relation with the intensity of primary production events. In summer, the high primary production events are associated with cold water filaments, whereas lower production periods are associated with warmer SSTs. It exists therefore a bias toward colder temperatures, due to a more important export of material at depth during upwelling events. This bias is less important in winter, since SSTs of nutrient rich upwelling filaments and offshore waters are more homogeneous.

In the case of simulation DELAY, considering the inertia of the temperature record in the coccolithophorid pool, phytodetritus alkenone-like temperature profiles are more homogeneous (Fig. 6d). The winter profile of phytodetritus temperature is constant from the surface to the bottom. In spring, summer and autumn, the phytodetritus alkenone-like temperatures at the surface are colder than the corresponding seasonal mean SSTs, with a maximum difference of 0.6°C in spring. For these three seasons, the phytodetritus temperature then decreases of maximum 0.6°C until ∼100 m. Below this depth, the temperatures are constant. Because the alkenone-like temperature record of the coccolithophores is changed only during their growing phase, it induces

Alkenone-like proxy record in the NW African upwelling

X. Giraud

EGU

EGU

inertia in the response of the record to water temperature variations. The alkenone-like temperature signal is smoothed by the lateral advection and vertical mixing of the coccolithophores. The coccolithophores at depth also have a warmer alkenone-like temperature record compared to simulation STD, because their growth rate is reduced
5 compared to the surface and they are mixed with pools coming from the warm superficial layers.

3.3.2.   Temperature record in sediments

Figure 7 shows the modelling results of alkenone-like IPT, model annual mean SST, and the difference between the two, for the reference simulation STD. The lowest IPT
10 are located on the continental shelf, north of Cape Blanc, with a minimum of 16.8°C. It then generally increases offshore. The area south of Cape Blanc is an exception, with a high IPT on the shelf, which we can associate to the particularly warm SSTs close to the coast. The map of temperature difference (Fig. 7, right) shows that the IPTs are colder than the annual mean SSTs, with an average difference of 1.6°C on
15 the modelling region.
    Table 3 shows the alkenone-derived temperature of core top sediments for different core sites off Mauritania, as well as the climatological annual mean SSTs, the modelled annual mean SSTs and the modelled alkenone-like IPT. The core locations are also shown on Fig. 1. It shows clearly that at the depth of core locations, between 750 m
20 and 3000 m, the modelled alkenone-like IPT are colder than the climatological annual mean SSTs by 1.1°C to 2.1°C. In contrast, the alkenone derived temperatures of core top sediments at these core locations, using the Müller et al. (1998) calibration, are similar or warmer than the annual mean SSTs.

4. Discussion

The processes potentially responsible for the temperature difference between the modelled alkenone-like IPT and the annual mean SSTs are (1) the depth of alkenone production, (2) the seasonality of the coccolithophores production, (3) the lateral advection and vertical transport of the phytodetritus, and (4) the resuspension and transport of sediments. If we introduce the possibility of inertia in the alkenone production (simulation DELAY), and therefore a delay in the response of the coccolithophores to the changing growing conditions, then the lateral advection of the coccolithophores at the surface may also play a role in the final sedimentary temperature record. We are going to discuss the influence of each of these aspects, and then discuss the implication on the interpretation of the alkenone-derived temperatures of the core top sediments.

4.1. Lateral advection and vertical transport of phytodetritus

The high and homogeneous sinking velocity set in the model (200 m d^{-1}) is responsible for a fast export of the organic matter (detritus pool of the model) from the surface to the sea floor. As a consequence, the lateral advection of particles in the water column seems to play a minor role in the temperature signal mixing. In order to evaluate this lateral advection component, we performed a sensitivity test, where the advection term applied to the detritus pool has been disabled. This test has little consequences on the biological distribution and primary production location, since the detritus pool is still remineralising progressively at depth, and sustains the correct nutrient recycling budget for the upwelling. The IPT obtained from this sensitivity test is similar to the reference simulation, with minor temperature variations, lower than 0.2°C (not shown). We therefore conclude that the lateral advection of the phytodetritus has no impact on the temperature signal when the sinking velocity is fast and homogeneous.

Nevertheless, some studies suggest that the vertical sinking velocities are low in the surface mixed layer and increase with depth, due to aggregation processes (Kriest and Evans, 1999; Berelson, 2002; Klaas and Archer, 2002; Kriest, 2002). A relatively low

EGU

sinking velocity in the surface layer would therefore favour a transport of the detritus pool by the lateral advection. This would lead to a most efficient transfer of particles produced in cold onshore waters toward most offshore locations, on the slope or in abyssal plain. Therefore, we performed a sensitivity case on the sinking rate, consider-
5 ing a sinking velocity of $5\,\mathrm{m\,d^{-1}}$ in the upper $50\,\mathrm{m}$, followed by an exponential increase up to $200\,\mathrm{m\,d^{-1}}$ to the bottom, with an increase scale of $200\,\mathrm{m}$.

The IPT produced by this lower sinking rate setting is different from the reference simulation only in the part south of $22°\,\mathrm{N}$ (not shown). There, the IPT is $\sim0.4°\mathrm{C}$ colder than for the reference simulation STD, with a maximum cooling of $1°\mathrm{C}$ in localized area.
10 That means that in this southern domain, the model IPT is between 1.5 and $3°\mathrm{C}$ colder than the annual mean SST. We conclude that the lower sinking rate has an impact in the region where SST gradients are stronger. The particulate material produced in the cold central upwelling area is advected offshore in the surface layer, and contributes to the sedimentation on the continental slope, where SSTs are already warmer. It seems
15 that in the northern part, this effect is negligible since the strong currents are mostly parallel to the slope, and therefore parallel to the general SST isotherms.

4.2. Sediment resuspension

Because of the distinction done in the model between detritus (D) and suspended sediments (S), it is possible to keep track of the direct detritus flux at the bottom, sep-
20 arately from the sediment resuspension and transport. It exists therefore a difference between the final sediment accumulation, and the time-cumulated flux of the detritus at the bottom. The comparison of the IPT and the alkenone-like temperature of the total phytodetritus bottom flux provides informations on the effect of the resuspension processes.
25 The resuspension of the sediments on the shelf did not modify the IPT on the slope in the reference simulation STD (not shown). Only small temperature differences ($<0.2°\mathrm{C}$) appear on the shelf due to local redistribution processes. Even if the actual parameterisation of the sediment resuspension participates to a better budget of the

X. Giraud

nutrients by enabling their remineralization in the water column, it does not influence directly the sediment temperature distribution. Nevertheless, considering the sedimentary temperature distribution (Fig. 7, left), with colder IPTs on the shelf, any effective sediment transport from the coast to the slope would participate to a cooling of the alkenone-like temperature signal of the slope sediments, and therefore to increase the temperature difference between annual mean SSTs and IPTs.

4.3. Seasonality

The seasonality of the coccolithophores has been shown on the Figs. 5 and 6. Considering the example of the vertical profiles at core location SU94-11S offshore Cape Blanc (Fig. 6), it appears that the coccolithophores concentration is twice as high in winter than in other seasons. Does this produce a seasonal bias in the IPT? Figure 8 shows, for the same core location, the vertical profiles of annual mean water temperature, annual mean phytodetritus alkenone-like temperature, and the mass-averaged annual mean phytodetritus alkenone-like temperature. The difference between the two profiles of phytodetritus alkenone-like temperatures is due to the relative weight of productive periods. At the surface and subsurface, the temperature difference is at maximum, between 0.6 and 0.8°C, depicting the winter influence as well as the cold, productive filaments in summer. Below ∼100 m, the temperature difference is small and constant until the bottom, ∼0.2°C. This is also the temperature difference obtained for the simulation DELAY (Fig. 8b). We consider therefore that the seasonality of coccolithophores production has a minor effect on the IPT in this particular location. It is worth to notice that Müller and Fischer (2001), based on a 4-year sediment trap record of alkenones at stations CB, offshore Cape Blanc, also concluded that the core-top sediments alkenone-based temperature was best correlated with the annual mean SST, but for a different reason. Although the alkenone production showed a strong seasonality, the seasonal flux variations were different for each year, leading to an averaged record in sediments.

4.4. Production depth

Since lateral advection of particles, sediment resuspension, and coccolithophore seasonality seem to play only a minor role in the production of the IPT, the temperature difference between the IPT and the annual mean SST has to be found in the production depth.

It appears clearly on the vertical profiles presented on Figs. 6 and 8 that the decrease of the phytodetritus alkenone-like temperature in the water column occurs mostly in the first 100 m, in relation with the progressive contribution of deeper, "colder" coccolithophores. Therefore a sensitivity test (simulation GROWTH) has been performed in order to evaluate the impact of growth depth of coccolithophores. This sensitivity case is based on a feature of *E. huxleyi* population: it is argued that *E. huxleyi* is disadvantaged at low light levels compared to other phytoplankton groups (Merico et al., 2004). This feature is specified in the model by a lower parameter for initial slope of the PI curve of the coccolithophorid PFT, set to $0.015 \, \text{W m}^{-2}$ instead of $0.025 \, \text{W m}^{-2}$. As a consequence, the growth rate of coccolithophores is lowered at depth, and the vertically integrated production may be deeply reduced. In order to compensate this effect, we also increased the specific maximum growth rate, set to $0.5 \, \text{d}^{-1}$ instead of $0.4 \, \text{d}^1$ for the reference simulation, so that coccolithophores are favoured in the ocean surface.

This new parameterisation of the coccolithophorid PFT leads to a slightly shallower coccolithophores distribution. At core location SU94-11S, ~70% of the coccolithophorid mass is now located in the upper 50 m, compared to ~60% in the reference simulation STD. But the increase of the maximum specific growth rate did not completely compensate the decrease of production at depth, so that the general coccolithophores concentrations are lower also at the sea surface.

The resulting IPT is slightly warmer than the reference simulation, which also means closer to the model annual mean SSTs. In a simulation combining this new coccolithophorid PFT parameterisation with the inertia in temperature adaptation of coccolithophores (simulation DELAY+GROWTH), the IPT is still ~1°C colder than the annual

EGU

Alkenone-like proxy record in the NW African upwelling

X. Giraud

mean SST (Fig. 9). This temperature difference is still significant since it appears to be systematic on the study domain. The reason is still a significant contribution of the coccolithophores populations present in the lower part of the MLD to the phytodetritus alkenone-like temperature record.

5   According to this last sensitivity case, it seems difficult to force the coccolithophore population to be localised only in the top 30 m without modifying the equilibrium with the other phytoplanktonic PFT. Regarded as the total coccolithophores population, the coccolithophorid PFT that we modelled is correctly distributed in time and space (horizontally and vertically). The question of the distribution of alkenone production in the

10   coccolithophore population itself appears therefore to be of primary importance. As already mentioned, the main alkenone producer species *E. huxleyi* can be present and be the main contributor to the coccolithophore assemblage down to 100 m or deeper. We think therefore that the implicit assumption done in the model, considering that total coccolithophores and *E. huxleyi* distributions can be assimilated, is correct.

15   The alkenone distribution in the surface ocean is most probably a question of physiological factors. The exact conditions of alkenone production, during the coccolithophores growth, are unfortunately not well known. Batch culture experiment have demonstrated that the alkenone cell content, as well as the Uk'37, may be significantly affected by environmental conditions like nutrient or light stress, as well as stationary or

20   exponential growth phases (e.g. Epstein et al., 1998; Prahl et al., 2003). The quantity of alkenone per cell may vary in function of growth conditions, and therefore be unequal from one living depth to another. In order to answer this question, we call for further studies of the physiological factors responsible for alkenone production.

4.5.   Calibration and interpretation of the Uk'37 index

25   As the alkenone-derived temperature of core top sediments are usually associated to the annual mean SSTs, the previous sections have tried to understand the reason why our model results always produce a temperature difference between IPTs and annual mean SSTs. We pointed out the importance of the production depth. As the coccol-

Title Page

Abstract   Introduction

Conclusions   References

Tables   Figures

◀   ▶

◀   ▶

Back   Close

Full Screen / Esc

Print Version

Interactive Discussion

EGU

ithophores distribution in the model seems correct, we concluded that the alkenone production itself may not be simply proportional to the coccolithophore biomass. Nevertheless the conditions of alkenone production are not well known, and our model may still correctly represent the distribution of alkenone distribution. In this section, we would like to comment the case where the model produces the correct IPT, and the meaning of its mismatch with the alkenone-derived temperatures.

For each core presented in Table 3, Fig. 10 shows the different temperatures obtained from alkenone measurements, climatic database and model simulations. It shows first that the annual mean SSTs from the model and Levitus (1994) data are similar, which confirms the good representation of the upwelling by the model. Despite the large geographical distribution of the cores (see Fig. 1), the annual mean SSTs do not vary much, and range between 19.8 and 20.9°C for the model results, and are even closer (between 20.1 and 20.7°C) for the Levitus (1994) data. These annual mean SSTs do not seem to show any clear relation with the alkenone ratio variations. Using the Müller et al. (1998) calibration, the Uk'37 variations for these cores represent alkenone derived temperatures ranging between 20.2 and 22.7°C. Nevertheless, it is important to notice that the standard error is estimated at ±1.5°C (Müller et al., 1998), which is represented on Fig. 10. Considering this error bar, the alkenone derived temperatures of the core top sediments are in agreement with the annual mean SSTs. An exception can be made for the two cores having the highest Uk'37. For these two cores, SU94-20bK (25°1 N, 16°9 W) and GIK12309-1 (26°0 N, 15°7 W), the alkenone derived temperatures are higher than the annual mean SSTs. The model IPTs associated to the cores presented in Table 3 and Fig. 10 show small variations, and range between 18.7 and 19.4°C. Therefore, they show the same trend as the annual mean SSTs, and they are 1.1 to 2.1°C colder than the latter.

As long as we consider the alkenone index calibration as correct, the mismatch between the alkenone derived temperature of core top sediments and the modelled IPT may come either from a missing process in the modelling approach, or a bad interpretation of the alkenone derived temperature.

The first missing process that we can invoke is a diagenetic modification of the alkenone ratio in the sediments. After the sediment burial, a differential degradation of di- and tri-unsaturated alkenone compounds may have lead to an increase of the Uk'37, corresponding to an apparent warming of the sediments alkenone-derived tem-
5 perature record. Some contradictory studies argue for a possible modification of the original temperature signal in the sediments (Hoefs et al., 1998; Gong and Hollander, 1999; Rontani et al., 2005), whereas other studies conclude that there is no diagenetic effect on the temperature record (e.g. Grimalt et al., 2000; Harvey, 2000). The diagenetic bias stays therefore only a hypothesis.

10 A second process that could explain the temperature mismatch would be a contamination by allochtonous material. Each location would be contaminated by allochthonous transported material having a relative warmer alkenone-derived temperature record. The model IPT would therefore represent the "cold" temperature of the autochthonous sedimentary flux, and the alkenone derived temperature the result of the
15 mixing with a "warm" component. The origin of this hypothetic "warmer" allochthonous material is hard to find since the only available sedimentary material would come from the continental shelf, which is an area where we expect the IPT to be colder.

Another explanation would be a miss-interpretation of the alkenone derived temperature, related to the age of the alkenone pool. Previous studies have shown that
20 the alkenones were 1000–4500 years and ∼1000 years older than the co-occurring foraminifera in the Namibian slope sediments (Mollenhauer et al., 2003) and Chilean margin sediments (Mollenhauer et al., 2005), respectively. But no age difference have been found between the alkenones and co-occurring foraminifera of a core in NW Africa (GeoB5546-2, 27.53°N, 13.73°W), just north of our study area (Mollenhauer
25 et al., 2005). Mollenhauer et al. (2005) suggest that the physical depositional settings, such as shelf width, or morphologic depressions, may play a role in the age control of the sediment components. The core GeoB5546-2, although in the NW Africa coastal upwelling system, is not facing a large continental shelf. In contrast, the cores presented in the Table 3 are facing a large continental margin, as it is for the Namibian

margin. It is therefore possible that the alkenones in these cores also present an age offset. If this would be the case, the alkenone derived temperature would refer to an averaged temperature over a certain past period, extending to the present day. The model IPT corresponds only to the present day characteristics of the alkenone sedi-
5 mentation. As the alkenone-derived temperatures are warmer than the model IPTs, that means that the present day alkenone pool would be mixed with a "warmer" and older alkenone pool. Appendix A presents an attempt to estimate past temperatures of the sedimentary fluxes, based on the assumption of an alkenone age offset, and a decreasing exponential law of contribution of former sediments to the core top. In the
10 case of the core SU94-11S, offshore Cape Blanc, the IPT at 6 ka BP is then estimated to be between 2.8°C and 5.7°C warmer than the present day IPT. These alkenone-like paleo-temperature reconstructions are conjectural, and call for a proof by measuring the age of the alkenones in slope sediments facing the large NW Africa continental shelf.

15 **5. Conclusions**

We developed a coupled physical-biogeochemical model to simulate the production, the transport and the sedimentation of an alkenone-like proxy in the context of the North-West African upwelling system, between 19° N and 27° N. We conclude that the alkenone-like temperature record of the slope sediments (between 1000 m and 3000 m)
20 should show a cooling between 1.1 and 2.1°C for the present day, compared to the annual mean SSTs. This result is in disagreement with the general use of the Uk'37 index, which is used to reconstruct annual mean SSTs. The temperature difference obtained in our model seems to be mostly due to the production depth of the coccolithophores, and to a minor contribution of seasonality and lateral advection. These
25 results are based on the assumption that the quantitative production of alkenones was proportional to the coccolithophores distribution in the water column. Our results are therefore calling for further studies on the alkenone production in the water column.

Appendix A

This appendix is an attempt to estimate the past temperature of sedimentary fluxes, based on the modelled IPT for the present day, the alkenone derived temperature of core top sediments, and assuming an age offset of the alkenone age with the co-
5 occurring foraminiferal. Our hypothesis is that the surface sediment alkenones are issued from a mixing with older alkenones.

Assumption #1: The relative contribution of each time period to the core top sediments, $\alpha_S(t)$, follow a decreasing exponential law as follow:

$$\alpha_S(t) = \frac{1}{\beta} \exp\left(-\frac{t}{\beta}\right) \tag{A1}$$

10 where t is the time BP (in ka), and β is the age offset of the core top alkenones (in ka). This assumption could be discussed in regard to the variation of primary productivity or sedimentary flux over the past period, as well as modifications in the mixing rate in the sediments. The present function is based on constant production and mixing rates. It also considers an infinite thickness of the sediments, which approximation facilitates
15 the calculation and justifies the use of the following integrations from 0 to infinity.

Let $A_S(t)$ the apparent age of the sediments, and $A_i(t) = t$ the age of the instantaneous sedimentary flux. We can verify that the apparent age of the core top sediments, $A_S(0)$ is equal to the age offset:

$$A_S(t = 0) = \int_0^\infty A_i(t)\,\alpha_S(t)\,dt = \int_0^\infty \frac{t}{\beta} \exp\left(-\frac{t}{\beta}\right) dt = \beta \tag{A2}$$

20 Let $T_S(t)$ the alkenone derived temperature of the sediments.

Let $T_i(t)$ the alkenone derived temperature of the instantaneous sedimentary flux, which is also the IPT.

The alkenone derived temperature of the core top sediments, $T_S(0)$, is the mass

weighted temperature accumulated over time, and can be expressed as follow:

$$T_S(0) = \int_0^\infty T_i(t)\,\alpha_S(t)\,dt \tag{A3}$$

Assumption #2: The IPT has evolved linearly over a certain past period (θ, in ka), and can be expressed as follow:

$$T_i(t) = T_i(0) + t\,\frac{T_i(\theta) - T_i(0)}{\theta} \tag{A4}$$

With Eqs. (A3) and (A4), we obtain:

$$T_S(0) = \int_0^\infty \left(T_i(0) + t\,\frac{T_i(\theta) - T_i(0)}{\theta}\right)\frac{1}{\beta}\exp\left(-\frac{t}{\beta}\right)dt \tag{A5}$$

$$T_S(0) = T_i(0)\int_0^\infty \frac{1}{\beta}\exp\left(-\frac{t}{\beta}\right)dt + \frac{T_i(\theta) - T_i(0)}{\theta}\int_0^\infty \frac{t}{\beta}\exp\left(-\frac{t}{\beta}\right)dt \tag{A6}$$

It can be easily demonstrated that:

$$\int_0^\infty \frac{1}{\beta}\exp\left(-\frac{t}{\beta}\right)dt = 1 \tag{A7}$$

and

$$\int_0^\infty \frac{t}{\beta}\exp\left(-\frac{t}{\beta}\right)dt = \beta \tag{A8}$$

Equation (A6) becomes:

$$T_S(0) = T_i(0) + (T_i(\theta) - T_i(0))\frac{\beta}{\theta} \tag{A9}$$

$$\frac{T_i(\theta) - T_i(0)}{\theta} = \frac{T_S(0) - T_i(0)}{\beta} \tag{A10}$$

Alkenone-like proxy record in the NW African upwelling

X. Giraud

Print Version

Interactive Discussion

EGU

This term can be replaced in Eq. (A4):

$$T_i(t) = T_i(0) + (T_S(0) - T_i(0)) \frac{t}{\beta} \qquad (A11)$$

Equation (A11) expresses the IPT at any time, $T_i(t)$, as a function of the present day IPT, $T_i(0)$, which is obtained by model simulations, the alkenone derived temperature of the core top sediments, $T_S(0)$, and the age offset of the core top alkenones.

Before to proceed to numerical applications, it is important to evaluate the relative contribution of the sediment pools according to their age. Let $R_S(t)$ the proportion of sediments younger than t contributing to the core top sediments.

$$R_S(t) = \int_0^t \alpha_S(t)\,dt = \int_0^t \frac{1}{\beta} \exp\left(-\frac{t}{\beta}\right) dt = 1 - \exp\left(-\frac{t}{\beta}\right) \qquad (A12)$$

Numerical application: Considering the core SU94-11S as an example, we have:

$T_i(0)$=18.9°C, issued from the modelled IPT,

$T_S(0)$=20.8°C, issued from the alkenone derived temperature of core top sediments.

If we assume an alkenone age offset of β4 ka, we obtain: T_i(6 ka)=21.75°C, with a contribution of R_S(6 ka)=78%. If we assume an alkenone age offset of β=2 ka, we obtain: T_i(6 ka)=24.6°C, with a contribution of R_S(6 ka)=95%.

These results show that the alkenone age offset, if any, and which is directly related to the degree of sediment mixing, is an important factor to estimate the past temperatures. As expected, the older the core top sediments, the warmer the temperature of past fluxes. In the case of the core SU94-11S, offshore Cape Blanc, Mauritania, the temperature difference between present day and 6 ka BP, can be estimated between 2.8°C and 5.7°C.

EGU

References

Benthien, A. and Müller, P. J.: Anomalously low alkenone temperatures caused by lateral particle and sediment transport in the Malvinas Current region, western Argentine Basin, Deep Sea Res. I, 47, 2369–2393, 2000.

5 Berelson, W. M.: Particle settling rates increase with depth in the ocean, Deep Sea Res. II, 49, 237–251, 2002.

Bijma, J., Altabet, M., Conte, M., Kinkel, H., Versteegh, G. J. M., Volkman, J. K., Wakeham, S. G., and Weaver, P. P.: Primary signal: Ecological and environmental factors – Report from Working Group 2, Geochem. Geophys. Geosyst., 2, Paper number 2000GC000051, 2001.

10 Blanke, B., Roy, C., Penven, P., Speich, S., McWilliams, J., and Nelson, G.: Linking wind and interannual upwelling variability in a regional model of the southern Benguela, Geophys. Res. Lett., 29, 2188, doi:10.1029/2002GL015718, 2002.

Blayo, E. and Debreu, L.: Adaptive mesh refinement for finite-difference ocean models: First experiments, J. Phys. Ocean., 29, 1239–1250, 1999.

15 Blom, G. and Aalderink, H.: Calibration of three resuspension/sedimentation models, Wat. Sci. Tech., 37, 41–49, 1998.

Bory, A., Jeandel, C., Leblond, N., Vangriesheim, A., Khripounoff, A., Beaufort, L., Rabouille, C., Nicolas, E., Tachikawa, K., Etcheber, H., and Buat-Ménard, P.: Downward particle fluxes within different productivity regimes off the Mauritanian upwelling zone (EUMELI program),
20 Deep Sea Res. I, 48, 2251–2282, 2001.

Brassell, S. C., Eglington, G., Marlow, I. T., Pflaumann, U., and Sarnthein, M.: Molecular stratigraphy: a new tool for climatic assessment, Nature, 320, 129–133, 1986.

Chai, F., Dugdale, R. C., Peng, T.-H., Wilkerson, F. P., and Barber, R. T.: One-dimensional ecosystem model of the equatorial Pacific upwelling system. Part I: model development and
25 silicon and nitrogen cycle, Deep Sea Res. II, 49, 2713–2745, 2002.

Conkright, M. E., Locarnini, R. A., Garcia, H. E., O'Brien, T. D., Boyer, T. P., Stephens, C., and Antonov, J. I.: World Ocean Atlas 2001: Objective Analyses, Data Statistics, and Figures, CD-ROM Documentation. National Oceanographic Data Center, Silver Spring, MD, 17 pp., 2002.

30 Conte, M. H., Eglinton ,G., and Madureira, L. A. S.: Long-chain alkenones and alkyl alkenoates as palaeotemperature indicators: their production, flux and early sedimentary diagenesis in the Eastern North Atlantic, in: Advances in Organic Geochemistry, edited by: Eckardt, C. B.

et al., 1991; Org. Geochem., 19, 287–298, 1992.

Conte, M. H. and Eglinton, G.: Alkenone and alkenoate distribution within the euphotic zone of the eastern North Atlantic: correlation with production temperature, Deep Sea Res. I, 40, 1935–1961, 1993.

5 Conte, M. H., Thompson, A., Lesley, D., and Harris, R. P.: Genetic and physiological influences on the alkenone/alkenoate versus growth temperature relationship in *Emiliana huxleyi* and *Gephyrocapsa oceanica,* Geochim. et Cosmochim. Acta, 62, 51–68, 1998.

da Silva, A. M., Young, C. C., and Levitus, S.: Atlas of surface marine data, vol.1-5, NOAA Atlas NESDIS 6-10, 1994.

10 Debreu, L.: Raffinement adaptatif de maillage et méthode de zoom – application aux modèles d'océan, Ph.D. Thesis, Université Joseph Fourier, Grenoble, 2000.

Debreu, L. and Vouland, C.: AGRIF: Adaptive Grid Refinement In Fortran, available on http://www-lmc.imag.fr/IDOPT/AGRIF/index.html, 2003.

Di Lorenzo, E., Miller, A. J., Neilson D. J., Cornuelle B. D., and Moisan J. R.: Modelling observed 15 California Current mesoscale eddies and the ecosystem response, Int. J. Remote Sensing, 25, 1307–1312, 2004.

Eppley, R. W., Rogers, J. N., and McCarthy, J. J.: Half-saturation constants for uptake of nitrate and ammonium by marine phytoplankton, Limn. and Ocean., 14, 912–920, 1969.

Epstein, B. L., D'Hondt, S., Quinn, J. G., Zhang, J., and Hargraves, P. E.: An effect of dissolved 20 nutrient concentrations on alkenone-based temperature estimates, Paleoceanography, 13, 122–126, 1998.

Epstein, B. L., D'Hondt, S., and Hargraves, P. E.: The possible metabolic role of C_{37} alkenones in *Emiliana huxleyi*, Org. Geochem., 32, 867–875, 2001.

Fernandez, E., Balch, W. M., Maranon, E., and Holligan, P. M.: High rates of lipid biosynthesis 25 in cultured, mesocosm and coastal populations of the coccolithophore *Emiliania huxleyi*, Mar. Ecol. Prog. Ser., 114, 13–22, 1994.

Fischer, G., Donner, B., Ratmeyer, V., Davenport, R., and Wefer, G.: Distinct year-to-year particle flux variations off Cape Blanc during 1988–1991: Relation to δ^{18}O-deduced sea-surface temperatures and trade winds, J. Marine Res., 54, 73–98, 1996.

30 Fütterer, D. K.: The modern upwelling record off Northwest Africa, in: Coastal Upwelling: Its Sedimentary Record, Part B: Sedimentary Records of Ancient Coastal Upwelling, edited by: Tiede, J. and Süess, E., 105–121, Plenum, New York, 1983.

Gabric, A. J., Garcia, L., Van Camp, L., Nykjaer, L., Eifler, W., and Schrimpf, W.: Offshore

export of shelf production in the Cape Blanc (Mauritania) giant filament as derived from coastal zone color scanner imagery, J. Geophys. Res., 98 (C3), 4697–4712, 1993.

Giraud, X., Bertrand, P., Garçon, V., and Dadou, I.: Modeling d15N evolution: First palaeoceanographic applications in a coastal upwelling system, J. Marine Res., 58, 609–630, 2000.

5 Giraud, X., Bertrand, P., Garçon, V., and Dadou, I.: Interpretation of the nitrogen isotopic signal variations in the Mauritanian upwelling with a 2D physical-biogeochemical model, Global Biogeochem. Cycles, 17, 1059, 2003.

Gong, C. and Hollander, D. J.: Evidence for differential degradation of alkenones under contrasting bottom water oxygen conditions: Implication for paleotemperature reconstruction,

10 Geochim. Cosmochim. Acta, 63, 405–411, 1999.

Gregg, W. W., Ginoux, P., Schopf, P. S., and Casey, N. W.: Phytoplankton and iron: validation of global three-dimensional ocean biogeochemical model, Deep Sea Res. II, 50, 3143–3169, 2003.

Grimalt, J. O., Rullkötter, J., Sicre, M. A., Summons, R., Farrington, J., Harvey, H. R., Goñi,

15 M., and Sawada, K.: Modifications of the C37 alkenone and alkenoate composition in the water column and sediment: Possible implications for sea surface temperature estimates in paleoceanography, Geochem. Geophys. Geosyst., 1, paper number 2000GC000053, 2000.

Haidar, A. T. and Thierstein, H. R.: Coccolithophore dynamics off Bermuda (N. Atlantic), Deep-Sea Res. II, 48, 1925–1956, 2001.

20 Harvey, H. R.: Alteration processes of alkenones and related lipids in water columns and sediments, Geochem. Geophys. Geosyst., 1, paper number 2000GC000054, 2000.

Herbert, T. D., Schuffert, J. D., Thomas, D., Lange, C., Weinheimer, A., Peleo-Alampay, A., and Herguera, J. C.: Depth and seasonality of alkenone production along the California margin inferred from a core top transect, Paleoceanography, 13, 263–271, 1998.

25 Hoefs, M. J. L., Versteegh, G. J. M., Rijpstra, W. I. C., de Leeuw, J. W., and Damste, J. S. S.: Postdepositional oxic degradation of alkenones: Implications for the measurements of palaeo sea surface temperatures, Paleoceanography, 17, 42–49, 1998.

IOC, IHO and BODC: Centenary Edition of the GEBCO Digital Atals, published on CD-ROM on behalf of the Intergovernmental Oceanographic Commission and the International Hy-

30 drographic Organization as part of the General Bathymetric Chart of the Oceans; British Oceanographic Data Center, Liverpool, 2003.

Kara, A. B., Rochford, P. A., and Hurlburt, H. E.: Naval Research Laboratory Mixed Layer Depth (NMLD) Climatologies, NRL Report No. NRL/FR/7330-02-9995, 26 pp., 2002.

Alkenone-like proxy record in the NW African upwelling

X. Giraud

EGU

Klaas, C. and Archer, D. E.: Association of sinking organic matter with various types of mineral ballast in the deep sea: Implications for the rain ratio, Global Biogeochem, Cycles, 16, 1116, doi:10.1029/2001GB001765, 2002.

Köbrich, M. I. and Baumann, K.-H.: Seasonal and interannual variability of coccolithophore
5   flux and species composition off NW Africa (Cape Blanc), J. Nannoplankton Res., 26, p. 68, 2004.

Kriest, I.: Different parameterizations of the marine snow in a 1D-model and their influence on the representation of marine snow, nitrogen budget and sedimentation, Deep Sea Res. I, 49, 2133–2162, 2002.

10   Kriest, I. and Evans T. E.: Representing phytoplankton aggregates in biogeochemical models, Deep Sea Res. I, 46, 1841–1859, 1999.

Lee K. E. and Schneider R.: Alkenone production in the upper 200 m of the Pacific Ocean, Deep Sea Res. I, 52, 443–456, 2005.

Le Quéré, C., Harrison, S. P., Prentice, I. C., Buitenhuis, E. T., Aumont, O., Bopp, L., Claus-
15   tre, H., Cotrim da Cunha, L., Geider, R., Giraud, X., Klaas, C., Kohfeld, K. E., Legendre, L., Manizza, M., Platt, T., Rivkin, R. B., Sathyendranath, S., Uitz, J., Watson, A. J., and Wolf-Gladrow, D.: Ecosystem dynamics based on plankton functional types for global ocean biogeochemistry models, Global Change Biology, 11(11), 2016–2040, doi:10.1111/j.1365-2486.2005.1004.x, 2005.

20   Levitus, S., and Boyer T. P.: World Ocean Atlas 1994, vol. 4: Temperature, NOAA Atlas NESDIS 4, 129 pp., 1994.

Levitus, S., Burgett, R., and Boyer, T. P.: World Ocean Atlas 1994, vol. 3: Salinity, NOAA Atlas NESDIS 3, 111 pp., 1994.

Marchesiello, P., McWilliams, J. C., and Shchepetkin, A.: Equilibrium structure and dynamics
25   of the California current system, J. Phys. Ocean., 33, 753–783, 2003.

Marlowe, I. T.: Lipids as palaeoclimatic indicators. Ph. D. thesis, Univ. Bristol, England, 1984.

Merico, A, Tyrrell, T., Lessard, E. J., Oguz, T., Stabeno, P. J., Zeeman, S. I., and Whitledge, T. E.: Modelling phytoplankton succession on the Bering Sea shelf: role of climate influences and trophic interactions in generating *Emiliana huxleyi* blooms 1997–2000, Deep Sea Res.
30   I, 51, 1803–1826, 2004.

Mittelstaedt, E.: The ocean boundary along the northwest African coast: Circulation and oceanographic properties at the sea surface, Prog. Oceanog., 26, 307–355, 1991.

Mollenhauer, G., Eglinton, T. I., Ohkouchi, N., Schneider, R. R., Müller, P. J., Grootes, P. M., and

Alkenone-like proxy record in the NW African upwelling

X. Giraud

EGU

Rullkötter, J.: Asynchronous alkenone and foraminifera records from the Benguela Upwelling System, Geochimica et Cosmochimica Acta, 67, 2157–2171, 2003.

Mollenhauer, G., Kienast, M., Lamy, F., Meggers, H., Schneider, R. R., Hayes, J. M., and Eglinton, T. I.: An evaluation of ^{14}C age relationship between co-occurring foraminifera, alkenones, and total organic carbon in continental margin sediments, Paleoceanography, 20, PA1016, doi:10.1029/2004PA001103, 2005.

Moore, J. K., Doney, S. C., Kleypas, J. A., Glover, D. M., and Fung, I. Y.: An intermediate complexity marine ecosystem model for the global domain, Deep Sea Res., 49, 403–462, 2002.

Moore, J. K., Doney, S. C., and Lindsay, K.: Upper ocean ecosystem dynamics and iron cycling in a global three-dimensional model, Global Biogeochem. Cycles, 18, GB4028, doi:10.1029/2004GB002220, 2004.

Morel, A.: Process studies in eutrophic, mesotrophic and oligotrophic regimes within the tropical northeast Atlantic, in: The Changing Ocean Carbon Cycle: A Midterm Synthesis of the Joint Global Ocean Flux Study, edited by: Hanson, R. B., Ducklow, H. W., and Field, J. G., Cambridge Univ. Press, New York, 338–374, 2000.

Müller, P. J., Kirst, G., Ruhland, G., von Storch, I., and Rosell-Melé, A.: Calibration of the alkenone paleotemperature index Uk'37 based on core-tops from the eastern South Atlantic and the global ocean (60° N–60° S), Geochimica et Cosmochimica Acta, 62, 1757–1722, 1998.

Müller, P. J. and Fischer, G.: A 4-year sediment trap record of alkenones from the filamentous upwelling region off Cape Blanc, NW Africa and a comparison with distributions in underlying sediments, Deep Sea Res. I, 48, 1877–1903, 2001.

Müller, P. J. and Fischer, G.: Global core-top calibration of UK37 (update), PANGAEA, doi:10.1594/PANGAEA.126662, 2003.

Oschlies, A. and Garçon, V.: An eddy-permitting coupled physical-biological model of the North Atlantic 1. Sensitivity to advection numerics and mixed layer physics, Global Biogeochem. Cycles, 13, 135–160, 1999.

Peterson, E. L.: Benthic shear stress and sediment condition, Aquacultural Engineering, 21, 85–111, 1999.

Prahl, F. G., Muehlhausen, L. A., Zahnle, D. L.: Further evaluation of long-chain alkenones as indicators of Paleoceanographic conditions, Geochemica Cosmochimica Acta, 52, 2303–2310, 1988.

Alkenone-like proxy record in the NW African upwelling

X. Giraud

Title Page

Abstract	Introduction
Conclusions	References
Tables	Figures

◀◀ ▶▶

◀ ▶

Back Close

Full Screen / Esc

Print Version

Interactive Discussion

EGU

Prahl, F. G., Wolfe, G. V., and Sparrow, M. A.: Physiological impacts on alkenone paleother-mometry, Paleoceanog., 18, 1025, doi:10.1029/2002PA000803, 2003.

Prahl, F. G., Popp, B. N., Karl, D. M., and Sparrow, M. A.: Ecology and biogeochemistry of alkenone production at station ALOHA, Deep Sea Res. I, 52, 699–719, 2005.

5 Ribbe, J. and Holloway, P. E.: A model of suspended sediment transport by internal tides, Cont. Shelf Res., 21, 395–422, 2001.

Röske, F.: An atlas of surface fluxes based on the ECMWF re-analysis – a climatological dataset to force global ocean general circulation models, Max Planck Institut f. Meteorologie, report 323, pp. 41, 2001.

10 Rontani, J. F., Bonin, P., Jameson, I., and Volkman, J. K.: Degradation of the alkenones and related compounds during oxic and anoxic incubation of the marine haptophyte *Emiliana huxleyi* with bacterial consortia isolated from microbial mats from the Camargue, France, Org. Geochem., 36, 603–618, 2005.

Sachs, J. P. and Anderson, R. F.: Fidelity of alkenone paleotemperatures in southern Cape

15 Basin sediment drifts, Paleoceanography, 18, 1082, doi:10.1029/2002PA000862, 2003.

Sawada, K. and Shiraiwa, Y.: Alkenone and alkenoic acid compositions of the membrane frac-tions of *Emiliana huxleyi*, Phytochem., 65, 1299–1307, 2004.

Schiebel, R., Zeltner, A., Treppke, U. F., Waniek, J. J., Bollmann, J., Rixen, T., and Hemleben, C.: Distribution of diatoms, coccolithophores and planktic foraminifers along a trophic gradi-

20 ent during SW monsoon in the Arabian Sea, Mar. Micropal., 51, 345–371, 2004.

Shchepetkin, A. F. and McWilliams, J. C.: A method for computing horizontal pressure-gradient force in an oceanic model with a non-aligned vertical coordinate, J. Geophys. Res. -Oceans, 108 (C3), 3090, doi:10.1029/2001JC001047, 2003.

Shchepetkin, A. F. and McWilliams, J. C.: The regional oceanic modeling system (ROMS): a

25 split-explicit, free-surface, topography-following-coordinate oceanic model, Ocean Modelling, 9, 305–404, 2005.

Sicre, M. A., Ternois, Y., Paterne, M., Boireau, A., Beaufort, L., Martinez, P., and Bertrand, P.: Biomarker stratigraphic records over the last 150 kyears off the NW African coast at 25° N, Organic Geochem., 31, 577–588, 2000.

30 Sicre, M. A., Ternois, Y., Paterne, M., Martinez, P., and Bertrand, P.: Climatic changes in the upwelling region off Cap Blanc, NW Africa, over the last 70 kyear: a multi-biomarker approach, Organic Geochemistry, 32, 981–990, 2001.

Sprengel, C., Baumann, K.-H., Henderiks, J., Henrich, R., and Neuer, S.: Modern coccol-

Title Page

Abstract | Introduction

Conclusions | References

Tables | Figures

◄ | ►►

◄ | ►

Back | Close

Full Screen / Esc

Print Version

Interactive Discussion

EGU

ithophore and carbonate sedimentation along a productivity gradient in the Canary Islands region: seasonal export production and surface accumulation rates, Deep-Seas Res., 49, 3577–3598, 2002.

Thomsen, L., van Weering, T., and Gust, G.: Process in the benthic boundary layer at the Iberian continental margin and their implication for carbon mineralization, Prog. in Ocean., 52, 325–329, 2002.

Tilstone, G. H., Miguez, B. M., Figueiras F. G., and Fermin, E. G.: Diatom dynamics in a coastal ecosystem affected by upwelling: coupling between species succession, circulation and biogeochemical processes, Mar. Ecology Prog. Series, 205, 23–41, 2000.

Volkman, J. K., Barrett S. M., Blackburn S. I., and Sikes E. L.: Alkenones in Gephyrocapsa oceanica: Implications for studies of paleoclimate, Geochim. Cosmochim. Acta, 59(3), 513-520, 1995.

Zhao, M., Eglinton, G., Haslett, S. K., Jordan, R. W., Sarnthein, M., and Zhang, Z.: Marine and terrestrial biomarker records for the last 35 000 years at ODP site 658C off NW Africa, Organic geochemistry, 31, 919–930, 2000.

Alkenone-like proxy record in the NW African upwelling

X. Giraud

Title Page

Abstract | Introduction

Conclusions | References

Tables | Figures

◄◄ | ►►

◄ | ►

Back | Close

Full Screen / Esc

Print Version

Interactive Discussion

EGU

Table 1. Parameters of the biological model.

Parameter	Symbol	Value	Unit
Phytoplankton coefficients			
Initial P-I curve	α	0.025	$(W\ m^{-2})^{-1}\ d^{-1}$
Photosynthetically active radiation	PAR	0.4	
Light attenuation due to water	k_w	0.04	m^{-1}
Light attenuation by phytoplankton	k_c	0.03	$m^{-1}(mmol\ m^{-3})^{-1}$
Maximum growth rate for P_1	a_1	0.6	d^{-1}
Maximum growth rate for P_2	a_2	0.4	d^{-1}
Growth rate parameters (for P_1 and P_2)	b	1.066	
	c	1.0	$(°C)^{-1}$
Half saturation constant for P_1	k_1	2.1	$mmol\ m^{-3}$
Half saturation constant for P_2	k_2	0.53	$mmol\ m^{-3}$
Specific mortality rate	μ_P	0.03	d^{-1}
Zooplankton coefficients			
Assimilation efficiency	γ_1	0.75	d^{-1}
Maximum grazing rate	g	1.0	
Prey capture rate	ε	1.0	$(mmol\ m^{-3})^{-2}\ d^{-1}$
Quadratic mortality	μ_z	0.2	$(mmol\ m^{-3})^{-1}\ d^{-1}$
Excretion	γ_2	0.03	d^{-1}
Detritus coefficients			
Remineralization rate	μ_D	0.05	d^{-1}
Suspended sediment coefficients			
Remineralization rate	μ_S	0.001	d^{-1}

EGU

Table 1. Continued.

Photosynthesis and grazing expressions	

Photosynthesis growth rate $\quad J_i(z,t,N) = \min\left(J_i(z,t), J_{i,\max}\frac{N}{k_i+N}\right)$

Growth rate without nutrient limitation $\quad J_i(z,t) = \frac{J_{i,\max}\alpha I(z,t)}{\sqrt{J_{i,\max}^2 + (\alpha I(z,t))^2}}$

Maximum growth rate $\quad J_{i,\max} = a_i b^{cT}$

Insolation $\quad I(z,t) = I(t)_{z=0}\exp\left(\frac{k_w + k_c \int_0^z (P_1+P_2)dz}{\sqrt{1-\left(\cos\theta/1.33\right)^2}}\right)$

Zooplankton maximum growth rate $\quad G(P_1+P_2) = \frac{g\varepsilon(P_1+P_2)^2}{g+\varepsilon(P_1+P_2)^2}$

where z is the depth (m), t is time, T is the water temperature (°C) and θ is the angle of incidence at noon (radian).

EGU

Table 2. PFTs growth parameters. k_i: Half saturation constant for nitrate uptake (mmol m^{-3}); a_i: maximum specific growth rate (d^{-1}).

References	diatoms		coccolithophores	
	k_1	a_1	k_2	a_2
Eppley et al. (1969)	1.9		≤ 0.5	
Moore et al. (2002)	2.5	3.0[a]	0.5	3.0[a]
Chai et al. (2002)		3.0[a]	0.5	2.0[a]
Gregg et al. (2003)	1	2.0[a]	0.5	1.5[a]
Le Quéré et al. (2005)	1.2	0.6 (2.1[b])	0.064	0.2 (0.7[b])
Buithenhuis (DGOM)	2.1	0.6 (2.1[b])	0.53	0.4 (1.4[b])
This study – reference simulation	2.1	0.6 (2.1[b])	0.53	0.4 (1.4[b])

[a] The parameter is scaled by the temperature function (see references).
[b] This value is calculated with the temperature function: a_i 1.066^T, with T=20°C.
[c] DGOM: Dynamic Green Ocean Model. Available online at http://lgmacweb.env.uea.ac.uk/green_ocean/.
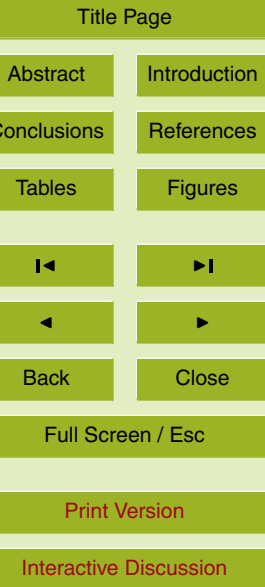
Table 3. Comparison between alkenone-derived SSTs, Levitus annual mean SSTs, model annual mean SSTs and model alkenone-like IPT, for core sites off the NW African margin (in °C). The SSTs from the Levitus atlas (Levitus, 1994), the $U_{37}^{k'}$ values measured in surface sediments, and the SSTs derived from alkenones using the Prahl et al. (1988) calibration are the one reported in Sicre et al. (2000).

Reference	Core site	Location		Depth (m)	Uk'37	SST (Uk'37)	SST (Levitus)	SST (model)	IPT (model)
Müller and Fischer (2003)	GIK12309-1	26°50 N	15°07 W	2849	0.79	22.7	20.3	20.8	18.8
"	GIK12326-3	23°18 N	17°25 W	1046	0.71	20.2	20.5	20.9	19.4
Sicre et al. (2000)	SU94-20bK	25°01 N	16°39 W	1445	0.77	22.0	20.4	19.9	18.7
"	SU94-21S	24°53 N	16°31 W	750	0.75	21.4	20.4	19.8	18.7
"	SU94-15S	23°44 N	17°16 W	1000	0.74	21.1	20.5	20.7	19.0
"	SU94-11S	21°29 N	17°57 W	1200	0.73	20.8	20.1	20.3	18.9
"	SU94-7S	21°11 N	18°52 W	3010	0.75	21.4	20.6	20.8	18.7
"	ODP 658A	20°75 N	18°58 W	2263	0.72	20.5	20.7	20.8	19.9

EGU

EGU
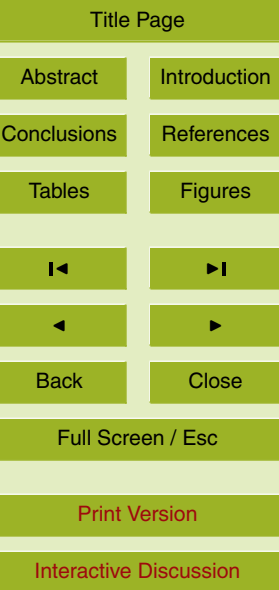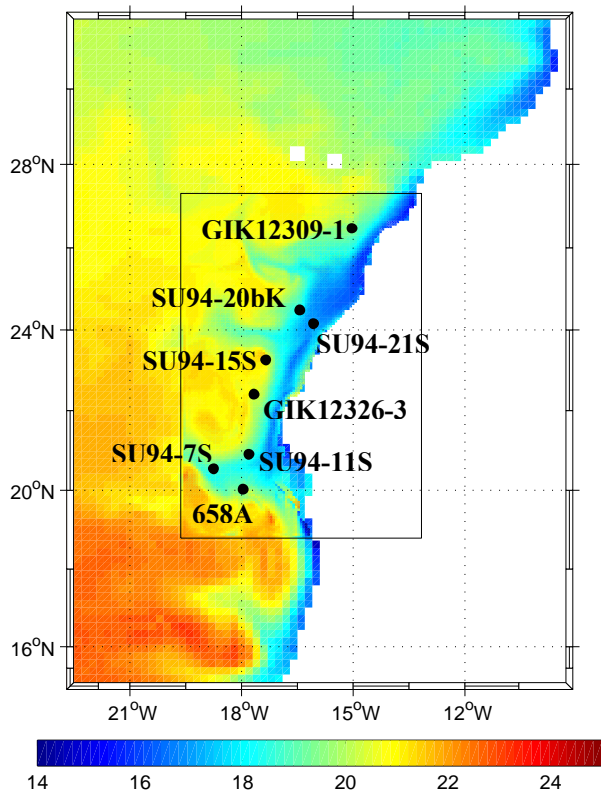
Fig. 1. SST (˚C) on the model domain at 1 June. The inner rectangle shows the extent of the child grid. The locations of the sedimentary cores are also indicated.
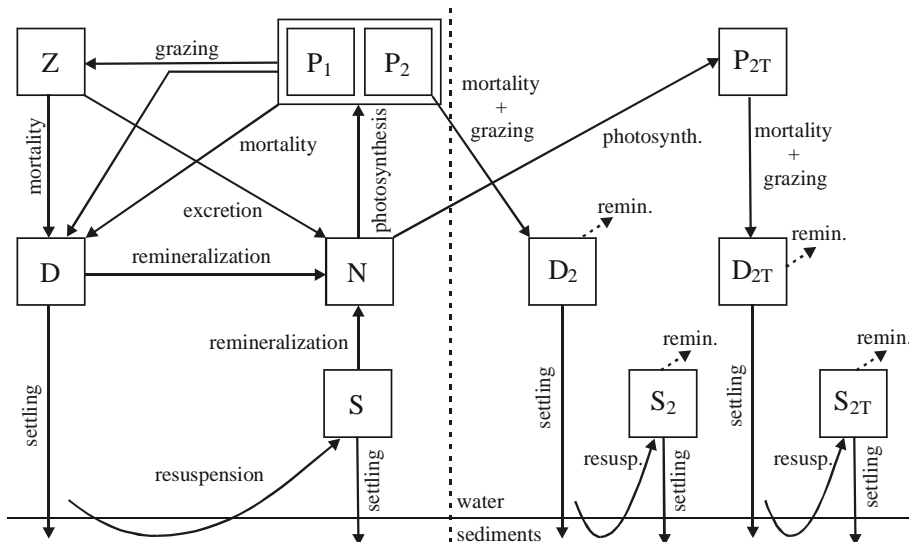
Fig. 2. Scheme of the biological model. The left hand part presents the basis of the trophic chain model. The right hand part contains the temperature related state variables. The dashed arrows shows non-conservative budget.
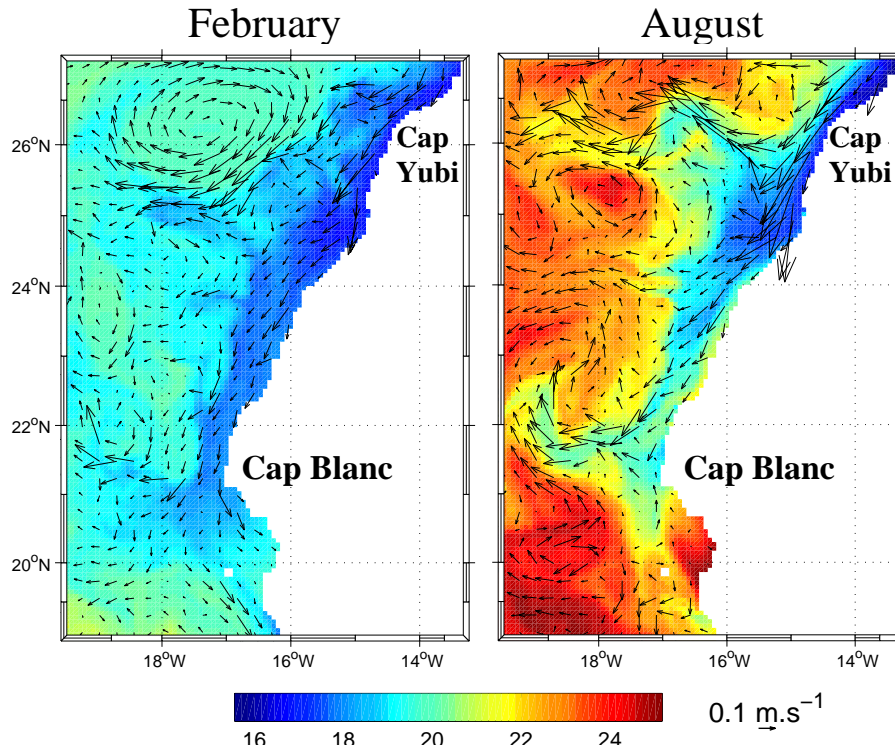
Fig. 3. Model SST (°C) and surface currents at 1 February (left) and 1 August (right), for the child domain.
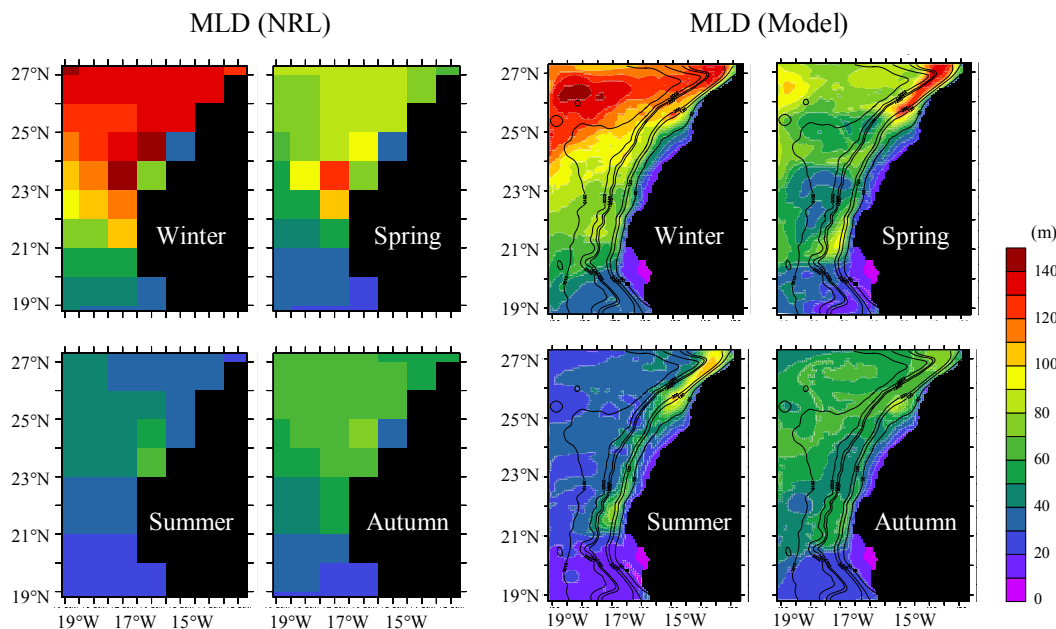
Fig. 4. Seasonal Mixed Layer Depth (MLD), in meters, from the Naval Research Laboratory monthly climatology (left) (Kara et al., 2002), and from the model (right).

EGU

EGU
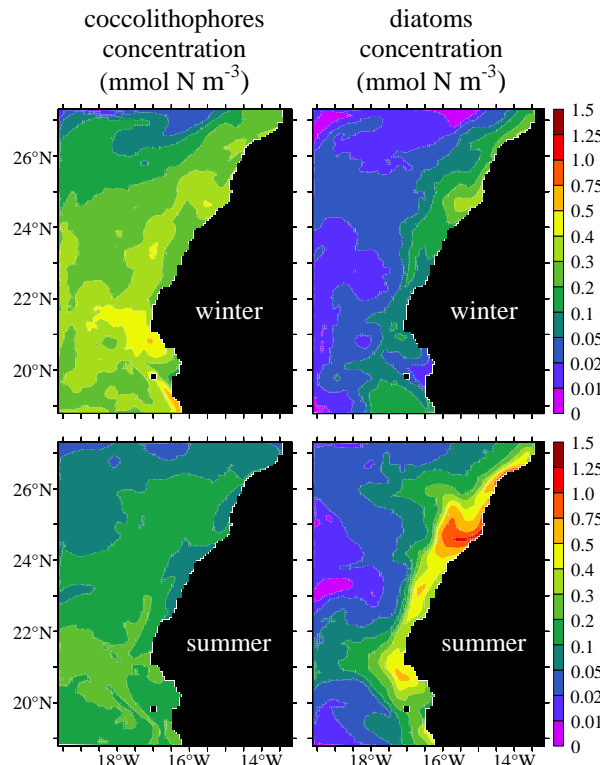
Fig. 5. Model distribution of coccolithophores (left col.) and diatoms (right col.) in winter (top) and summer (bottom) at the sea surface, in mmol N m^{-3}.
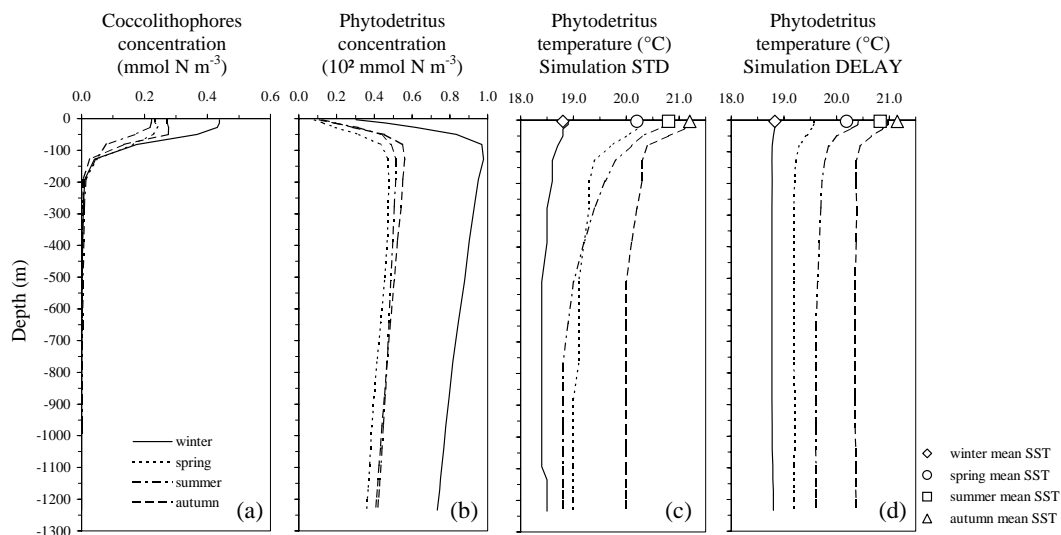
Fig. 6. Seasonal depth profiles at core location SU94-11S: model results for the coccolithophores concentration **(a)**, phytodetritus concentration **(b)**, and phytodetritus alkenone-like temperature for the reference simulation STD **(c)**, and simulation DELAY **(d)**. Seasonal profiles of winter (solid line), spring (dotted line), summer (dashed-dotted line) and autumn (dashed line). On (c) and (d) are also presented the model seasonal mean SSTs.

Title Page

Abstract | Introduction

Conclusions | References

Tables | Figures

◀◀ | ▶▶

◀ | ▶

Back | Close

Full Screen / Esc

Print Version

Interactive Discussion

EGU

EGU
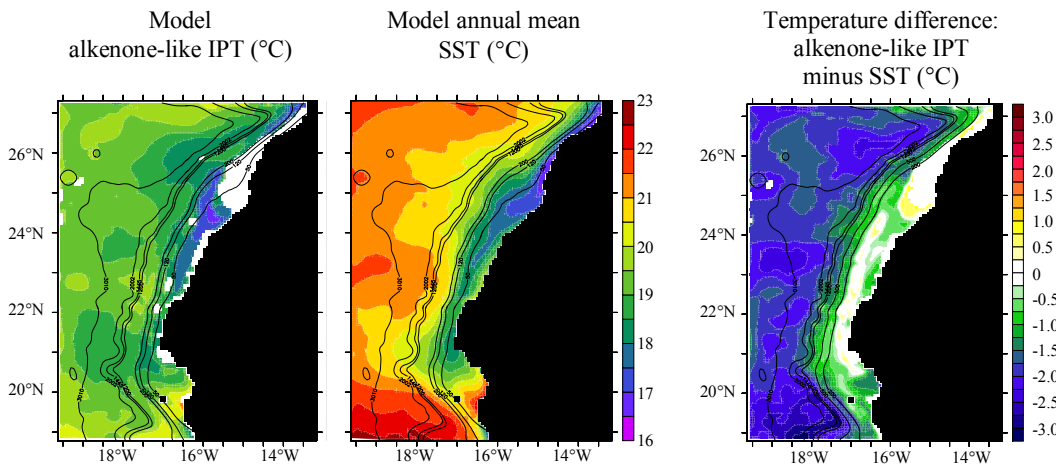
Fig. 7. Model results (reference simulation STD) of the alkenone-like IPT (left), annual mean SST (centre), and annual mean SST minus alkenone-like IPT (right), in °C. Solid lines show the bathymetry with isobath at 50, 120, 200, 1200, 1445, 2000, and 3000 m.
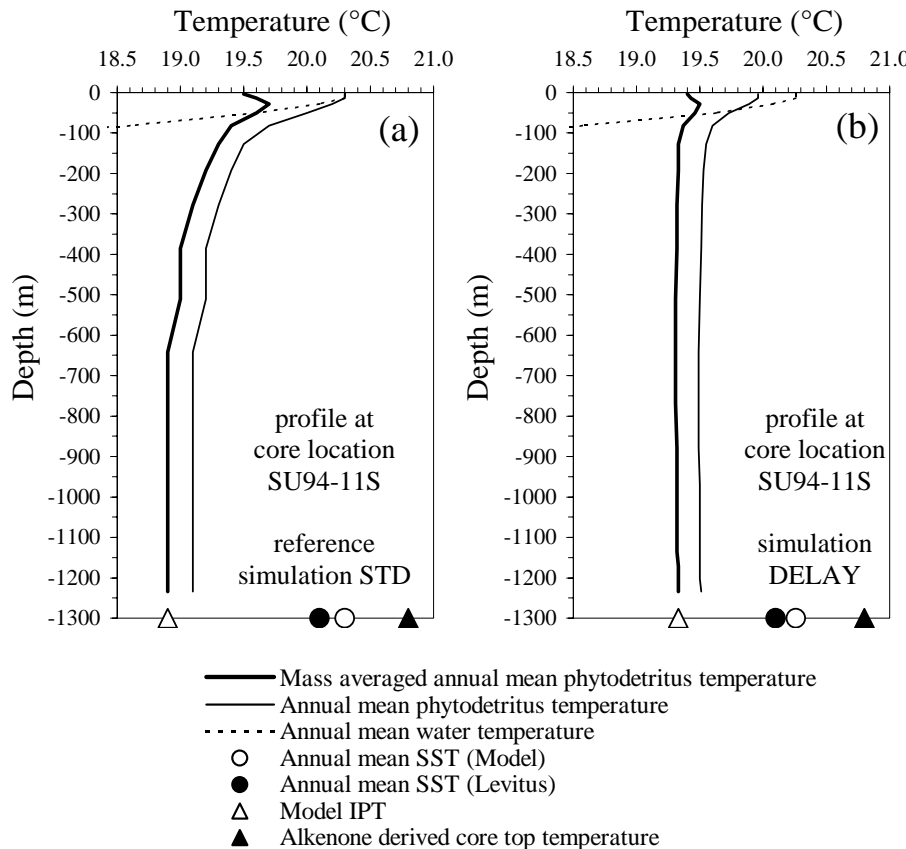
Fig. 8. Vertical profiles of model results for annual mean water temperature (dotted line), annual mean phytodetritus alkenone-like temperature (thin solid line) and mass averaged annual mean phytodetritus alkenone-like temperature (thick solid line) at core location SU94-11S for the reference simulation STD **(a)** and for simulation DELAY **(b)**.

EGU

Temperature difference:
alkenone-like IPT
minus SST (°C)
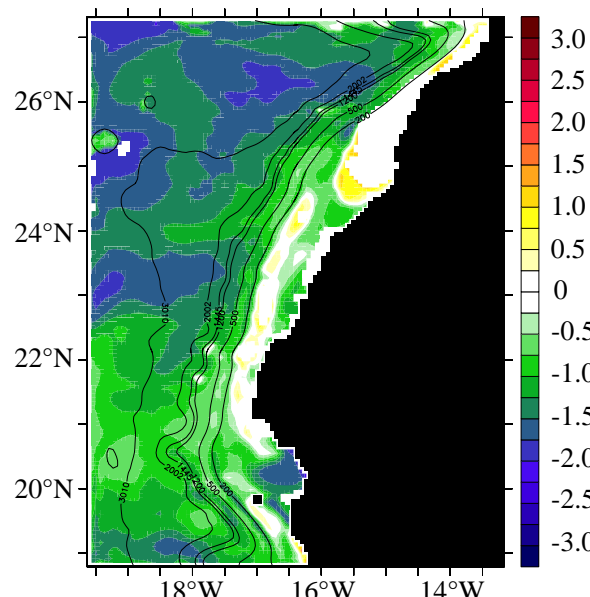
Fig. 9. Temperature difference between the alkenone-like IPT and the model annual mean SST, for simulation DELAY+GROWTH (combining the lower parameter for the initial slope of the PI curve of coccolithophores PFT and the inertia in temperature adaptation of coccolithophores).
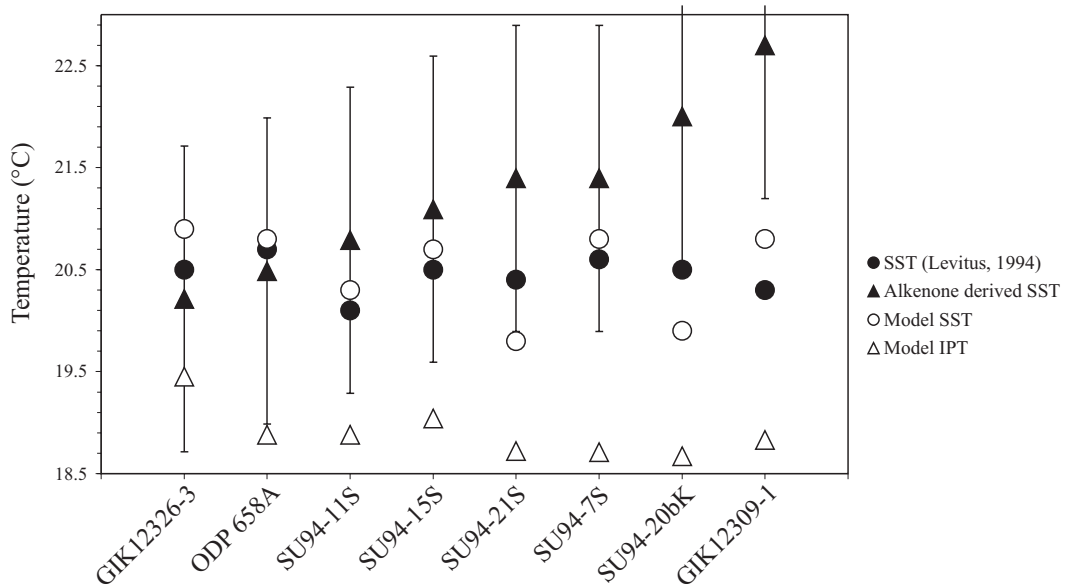
Fig. 10. Annual mean SSTs and sedimentary alkenone-derived temperature records for the cores presented in Table 3: Alkenone derived temperatures of core-top sediments using the Müller et al. (1998) global calibration (black triangles), assuming an error bar of ±1.5°C; annual mean SSTs from Levitus and Boyer (1994) (black circles, and linear regression as a solid line); model annual mean SSTs (white circles, and a linear regression as a dotted line); model (reference simulation STD) alkenone-like IPT (white triangles, and a linear regression as a dashed line). Cores are ordered by increasing alkenone index Uk'37 reported in Table 3.